Featured in Physics

Slow Quasiparticle Dynamics and Anyonic Statistics in a Fractional Quantum Hall Fabry-Pérot Interferometer

Noah L. Samuelson,[1,*] Liam A. Cohen,[1,*] Will Wang,[1] Simon Blanch,[1] Takashi Taniguchi,[2] Kenji Watanabe,[3] Michael P. Zaletel,[4,5] and Andrea F. Young[1,†]

[1]Department of Physics, University of California at Santa Barbara, Santa Barbara, California 93106, USA
[2]International Center for Materials Nanoarchitectonics, National Institute for Materials Science, 1-1 Namiki, Tsukuba 305-0044, Japan
[3]Research Center for Functional Materials, National Institute for Materials Science, 1-1 Namiki, Tsukuba 305-0044, Japan
[4]Department of Physics, University of California, Berkeley, California 94720, USA
[5]Material Science Division, Lawrence Berkeley National Laboratory, Berkeley, California 94720, USA

(Received 11 July 2025; revised 10 October 2025; accepted 8 January 2026; published 23 March 2026)

Anyons are two-dimensional particles with fractional exchange statistics that emerge as elementary excitations of fractional quantum Hall phases. Experimentally, their exchange statistics can be measured in the edge-state Fabry-Pérot interferometer, wherein the presence of N_{qp} localized anyons contributes a phase $N_{qp}\theta_a$ to the interference pattern where θ_a is twice the exchange phase. Here we report the observation of large, hysteretic phase jumps in a monolayer graphene Fabry-Pérot interferometer at $\nu = 1/3$. When the filling factor is increased from $\nu < 1/3$ toward the center of the plateau, we observe phase slips with magnitude $\Delta\theta \approx 2\pi/3$, consistent with the addition of individual quasiparticles to the interferometer bulk. These phase slips occur as instantaneous jumps in the interference signal, with intervals between the jumps indicating quasiparticle equilibration times exceeding 20 min. We use this long timescale to investigate the effect of changes in interferometer area A_I and N_{qp} independently at fixed magnetic field, revealing a striking memory effect in the phase slip magnitude. In particular, as the $\nu = 1/3$ plateau is approached from higher filling, we observed phase slips with $\Delta\theta$ significantly larger than $2\pi/3$ over the same range of gate voltage where quantized jumps are seen for increasing ν. We discuss this asymmetry in terms of bulk-edge coupling of quasiparticles localized near the edge or in the bulk, and argue that this effect can be qualitatively reconciled with theoretical expectations for strongly interacting quasiparticles in the presence of weak disorder and strongly nonequilibrium charge dynamics. Besides providing a replication of interferometric measurements sensitive to θ_a, our results highlight the key role played by charge dynamics on signatures of the anyon phase, and demonstrate that fractional quasiparticles can be indefinitely localized in nonequilibrium configurations.

DOI: 10.1103/fwjg-mx9h

Subject Areas: Condensed Matter Physics, Graphene, Quantum Physics

I. INTRODUCTION

When an Abelian anyon is brought along a closed trajectory encircling N_{qp} localized anyons, its wave function accumulates a phase

$$\frac{\theta}{2\pi} = \frac{e^*}{e}\frac{A_I B}{\Phi_0} + N_{qp}\frac{\theta_a}{2\pi}, \tag{1}$$

where A_I is the area of the loop, B is the applied magnetic field, θ_a is twice the exchange phase, and e^* is the quasiparticle charge [1–6]. Quantum Hall edge-state Fabry-Pérot interferometers exploit the contrast between localized anyons in the bulk and propagating anyonic quasiparticles along the chiral edge modes to directly observe this phase [7–10]. In a Fabry-Pérot interferometer, delocalized quasiparticles enter the cavity via a quantum point contact (QPC) and propagate along the edge to a second QPC; they can then exit the cavity immediately or complete an integer number of additional circuits before exiting. Trajectories differing by the number of circuits give an interference contribution to the conductance δG that is periodic in θ and can be measured as a function of B, A_I, or N_{qp}. The clearest signature of anyonic statistics is expected if N_{qp} changes

*These authors contributed equally to this work.
†Contact author: andrea@physics.ucsb.edu

Published by the American Physical Society under the terms of the Creative Commons Attribution 4.0 International license. Further distribution of this work must maintain attribution to the author(s) and the published article's title, journal citation, and DOI.

discretely while keeping A_I and B fixed; the resulting jump in θ then gives θ_a directly.

Fabry-Pérot interferometers have been investigated in GaAs heterostructures for nearly two decades [11–21]. These experiments have revealed that Coulomb interactions complicate the naive interpretation that a jump in θ entirely arises from the anyonic exchange phase [10]. Specifically, as charge enters the bulk of the interferometer, Coulomb repulsion may cause a change in A_I, leading to an observable phase shift even for fermionic quasiparticles. If the "bulk-edge coupling" is large, this change in the Aharonov-Bohm phase can completely obscure the contribution of θ_a. Recently, a breakthrough in the design of GaAs heterostructures led to the observation of phase shifts that agree quantitatively with the expected $\theta_a = 2\pi/3$ in the $\nu = 1/3$ state [18–20,22]. Graphene heterostructures are a natural venue in which to extend these results owing to the large fractional quantum Hall energy gaps observed at both odd- [23–26] and even-denominator filling factors [27–31]. Moreover, the nearby graphite gates in typical dual-gated geometries ensure a high degree of screening, suppressing bulk-edge coupling. Indeed, measurements of Fabry-Pérot interferometers in graphene have uniformly observed Aharonov-Bohm dominated interference in both integer and fractional filling factors [32–37].

II. FABRY-PÉROT INTERFERENCE IN $\nu = 1/3$

In this work, we study a monolayer graphene gate-defined Fabry-Pérot interferometer, shown schematically in Fig. 1(a). The interferometer is fabricated using anodic oxidation lithography to define the gate structure in a graphite layer. Dry van der Waals assembly techniques are then used to form a device with six separately gated regions [38]. In our device [Fig. 1(a)], two pairs of gates (NE/SE and NW/SW) define QPCs, while a plunger gate (P) provides additional control over the interferometer area. The center gate (C) and a global graphite bottom gate are used, together, to set the filling factor and, through fringe electric fields, adjust the transmission through the QPCs. All data are measured in a dry dilution refrigerator with a base temperature of 17 mK. Transport data at $B = 9$ T as a function of a common voltage applied to all six top gates in Fig. 1(b) show well-developed plateaus at filling factor $1/3$ and $2/3$. We operate our interferometer within the $1/3$ plateau at the indicated point at $B = 9$ T. We measure the transmission through the interferometer via the diagonal conductance, $G_D \equiv I_{\text{out}}/(V_+ - V_-)$ [see Fig. 1(a)]. To confirm that our experiment is probing chiral edge modes of the $1/3$ state, we measure the source-drain bias dependence of the two QPCs in the partial transmission regime individually. As shown in Fig. 1(c), both show strong suppression of G_D at low bias, as expected for tunneling between chiral Luttinger liquids at the QPCs [39–46]. This behavior is neither expected nor observed in the integer quantum Hall regime (see Supplemental Material [47] for a comparable measurement in the $\nu = 2$ state, showing no zero-bias suppression).

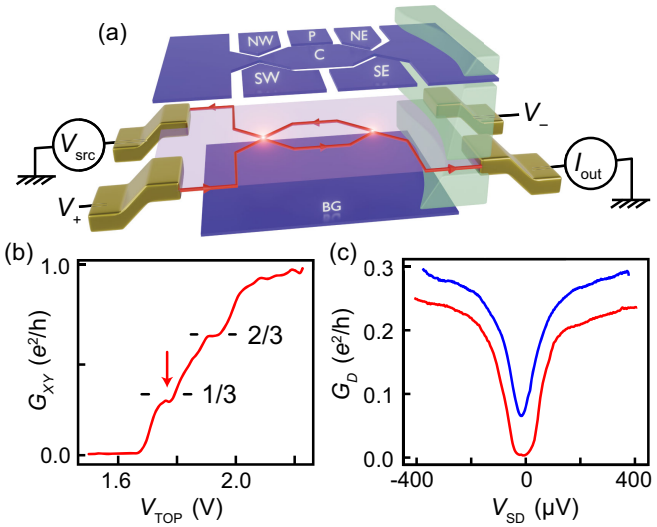

FIG. 1. Device schematic and characterization in the $\nu = 1/3$ state. (a) Schematic of the dual-graphite gated edge state Fabry-Pérot interferometer. The gates defining the interferometer are labeled C, NW, SW, NE, SE, and P. Edge states are formed in the monolayer graphene around the C-gated region and enter the interferometer via two QPCs tuned by the NW/SW and NE/SE gates. There is also a global graphite back gate (BG). (b) Hall conductance G_{XY} measured on the west side of the device as a function of the voltage V_{TOP} applied to all top gates together, with a fixed back gate voltage $V_{\text{BG}} = -1.5$V at $B = 9$ T and $T = 18$ mK. (c) Conductance through each QPC vs the dc source-drain bias V_{SD} (applied as an added voltage on the source electrode), with the $V_{\text{BG}} = -2.0$V throughout. The blue trace was taken with the C/P/NW/SW regions at filling $1/3$ ($V_{\text{C/P/NW/SW}} = 2.232$ V), and the NE/SE regions depleted ($V_{\text{NE/SE}} = -4.1$V). The red trace was taken with the NE/SE regions at filling $1/3$ ($V_{\text{C/P/NE/SE}} = 2.232$ V) and the NW/SW regions depleted ($V_{\text{NW/SW}} = 0.5$ V).

Figure 2(a) shows G_D at $\nu = 1/3$ with both QPCs set to partial pinch-off as a function of V_{P} and B (QPC operating set points are shown in Supplemental Material [47]). The interference shows high-visibility oscillations with lines of constant phase having a negative slope in the V_{P}-B plane, consistent with an Aharonov-Bohm dominated interference phase [10]. Following Eq. (1), we estimate the effective interferometer area to be $A_I = 3\Phi_0/\Delta B = 0.69$–$0.83$ μm^2 based on the $\Delta B \approx 15$–18 mT field period of the oscillations. This agrees with the nominal device area of $0.74 - 0.83$ μm^2 of the patterned graphite gates (see Supplemental Material for a more detailed analysis of the magnetic field period [47]). Estimates of the edge state velocity [47] give $v = 6.2 \pm 0.2 \times 10^4$ m/s, comparable to prior estimates for integer quantum Hall edge states in graphene [32,33,35,48]. We also characterize the visibility of Aharanov-Bohm interference at $\nu = 1/3$ as a function of

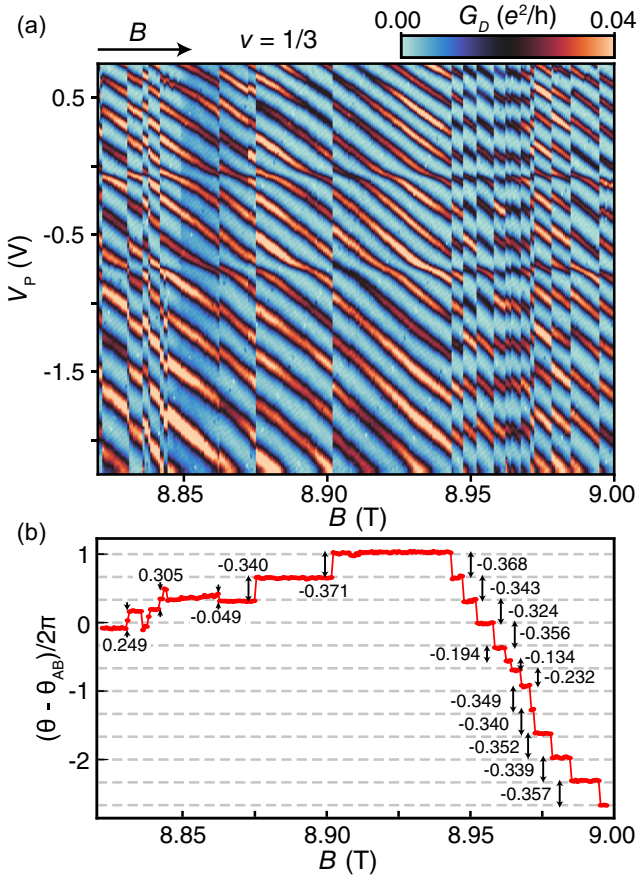

FIG. 2. Fabry-Pérot interference at $\nu = 1/3$. (a) G_D measured across the interferometer at $\nu = 1/3$, with both QPCs partially transmitting. The magnetic field is swept from low to high. (b) The phase extracted from the Fourier transform of the data in (a). A continuous Aharonov-Bohm phase is subtracted, and we adopt the convention $\Delta\theta \in (-\pi, \pi)$.

temperature where we extract a characteristic temperature scale $T_0 = 87$ mK (see Supplemental Material [47]).

In addition to the continuously tuned Aharonov-Bohm phase giving rise to the negative slope, the most striking feature of Fig. 2(a) is the presence of "hard" phase slips, where the interference phase changes instantaneously with respect to the 30-sec measurement time of each individual V_P trace, resulting in an apparent discontinuity between traces taken at subsequent magnetic fields. We also observe two clear "soft" phase slips, located at $V_P = -0.1$V and $V_P = -0.8$V, which are tuned continuously with V_P. These phase slips are nearly horizontal in the V_P-B plane, indicating a strong degree of capacitive coupling to the plunger gate likely from a localized defect state near the interferometer boundary. Defects of this type have been investigated in the integer quantum Hall regime in a previous work [49]. Here we focus on the hard phase slips which constitute the majority of the observed events.

To quantify the magnitude of the phase slips, we compute the Fourier transform of G_D with respect to V_P (over the range $V_P \in [-2.25\text{V}, -0.78\text{V}]$ in order to avoid the effect of the soft phase slips) for each value of B and extract the phase of the largest-magnitude peak, which determines the oscillation phase θ. Per Eq. (1), θ is expected to contain both a smoothly varying Aharonov-Bohm contribution as well as discrete contributions proportional to N_{qp}. The latter term includes the anyon double-exchange phase, as in Eq. (1), as well as the effect of bulk-edge coupling, which induced N_{qp}-dependent shifts in A_I [10]. To isolate the N_{qp}-dependent terms, we take a running trimmed mean of the line-by-line phase differences and subtract it from the measured phase (see Supplemental Material [47]).

The residual phase, $\theta - \theta_{AB}$, is plotted in Fig. 2(b). As this determines only the phase difference modulo 2π, we adopt the convention $\Delta\theta \in (-\pi, \pi)$. The magnitude of each phase slip is calculated from the difference in average value between intervals of stable phase. The statistical error in the phase slip measurements is small; repeated measurements within a single interval of stable phase show a standard deviation of $\sigma_\theta \approx 0.012 \times 2\pi$. A larger source of error arises from the fact that the oscillations are not perfectly periodic in V_P, generating different values of θ for different components of the Fourier transform. We estimate that this error may be as high as $\pm 2\pi \times 0.04$ (see Supplemental Material [47]). Most of the marked phase slips are consistent, within this uncertainty, with $\Delta\theta = \pm 2\pi/3$.

In GaAs, observed phase slips are always soft: they evolve continuously with both B and gate voltage [19]. This is consistent with an equilibrium picture in which quasiparticles move between the interior and exterior of the interferometer loop on timescales much faster than the integration time of the measurement. Our observation in Fig. 2(a) of hard slips, which appear instantaneous on measurement timescales, is not consistent with this picture, instead implying that quasiparticle dynamics are irreversible. This is observed directly in Figs. 3(a) and 3(b), where we contrast interference plots taken as a function of increasing and decreasing B. In these plots, V_P is fixed while V_C is swept rapidly to vary the interferometer area and produce an interference pattern, while B is ramped from minimum to maximum over 33 min. In Fig. 3(a), a series of discrete slips are observed. However, phase slips do not occur until the magnetic field has already been increased by 70 mT, nearly 20 min after the beginning of the measurement.

Reversing the direction of the B sweep [Fig. 3(b)] reveals a hysteretic behavior where phase slips start only after the field is *lowered* sufficiently. Evidently, the location of a given phase slip in our experiment is not an equilibrium property, but depends on the history of the system. Notably, the Aharonov-Bohm phase at the beginning of the measurements in both Figs. 3(a) and 3(b) evolves through several periods as a function of B. This implies that the magnetic flux through the interferometer changes by

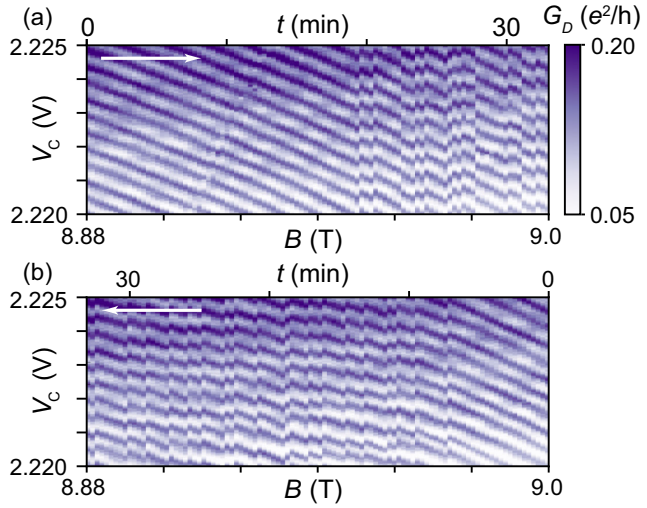

FIG. 3. Magnetic field hysteresis. (a) G_D vs V_C as the magnetic field is swept from 8.88 to 9 T. The latter half of the measurement shows many sudden phase jumps, beginning at $B = 8.95$ T and continuing until the end of the sweep. (b) G_D vs V_C as the magnetic field is swept from 9 to 8.88 T. The hard phase slips differ in exact location as compared to (a); in particular, they do not begin until $B < 8.97$ T and then continue until the end of the sweep at $B = 8.88$ T.

several quanta at fixed anyon charge and approximately fixed size, despite it being energetically favorable to add a quasihole to the bulk with each added flux quantum.

This hysteretic, sudden phase slip behavior is distinct from the three-state random telegraph noise observed in a parallel work studying a similar dual-gated graphene interferometer [37]. There, phase slips occur indefinitely as a function of time even when the magnetic field and gate voltage are fixed, indicating fluctuations in the number of anyons while the system remains close to equilibrium. In our experiment, no phase slips occur when the gate voltage and magnetic field are held fixed over timescales of hours, or even when they are swept over a sufficiently small range (see Supplemental Material [47]).

The picture in Fig. 3 can be at least partially understood as a consequence of exceptionally slow charge dynamics. As illustrated in Fig. 4, slow charging leads to a discrepancy between the equilibrium value of the compressible edge-state chemical potential μ_{edge}, which is set by the gate voltages and magnetic field and directly determines the area of the interference cavity, and the actual chemical potential of the graphene layer $\mu_{\text{bulk}}(t)$. The value of $\mu_{\text{bulk}}(t)$ requires quasiparticle trapping sites to be filled to equilibrate; if the trapping sites are sufficiently separated from the edge by the incompressible quantum Hall bulk, tunneling events may take minutes to hours to occur after it becomes energetically favorable to do so.

In a previous experiment on a device of nearly identical construction, we investigated the effects of slow charging in the integer quantum Hall regime. There, the observed phase slips (which in that case arise entirely from bulk-edge coupling) originated from a well-understood equilibrium charging picture, but became sudden-in-time and hysteretic as we continuously adjusted the dynamical barrier to charging the bulk with density and magnetic field [49]. Thus, while it is remarkable to see this effect at the single fractional quasiparticle level, its occurrence is not completely unexpected. Long charging times are a characteristic of quantum Hall systems [50,51], particularly in similarly fabricated graphene devices which boast low disorder and larger energy gaps for quantum Hall states compared to competing platforms, such as GaAs quantum wells [52].

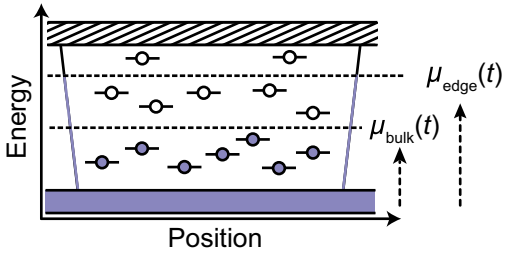

FIG. 4. Irreversible charging dynamics. Localized states within the fractional quantum Hall energy gap have slow tunneling rates to the gapless edge; as a result, the chemical potential of the electrically isolated bulk (μ_{bulk}) lags the chemical potential of the edge (μ_{edge}) during a ramp of the magnetic field or gate voltage. In this schematic, purple indicates filled states.

While slow charge dynamics naturally explains the phase-slip-free Aharanov-Bohm evolution we observe in the beginning of Figs. 3(a) and 3(b), it is important to note that the number of sharp phase slips observed in the upward field sweep is significantly fewer than the number in the reversed field sweep. This must indicate that some trapping sites filled during the measurement of Fig. 3(a) are never depopulated during the measurement taken in Fig. 3(b). This hysteresis implies the charging and discharging times must be different from each other, and begs the question what the broader consequences of such memory effects may be on the phase slip phenomenology.

III. MEMORY EFFECT AND ANOMALOUS PHASE SLIP MAGNITUDES

The long charging time allows us to measure the phase slips systematically at *fixed* magnetic field, eliminating any change in cavity area not a direct result of ΔN_{qp}. This is accomplished by modulating a single gate voltage faster than the charging time over a small range that nevertheless allows us to measure the interference phase, and then slowly varying the center of that gate voltage range to increment N_{qp}. Figure 5(a) shows data taken in this way at $B = 9$ T as a function of V_C. In this measurement, V_C is swept over a range spanning roughly 10 oscillations in approximately 30 sec. The range is adjusted from trace to trace, so that the average value of V_C increments slowly

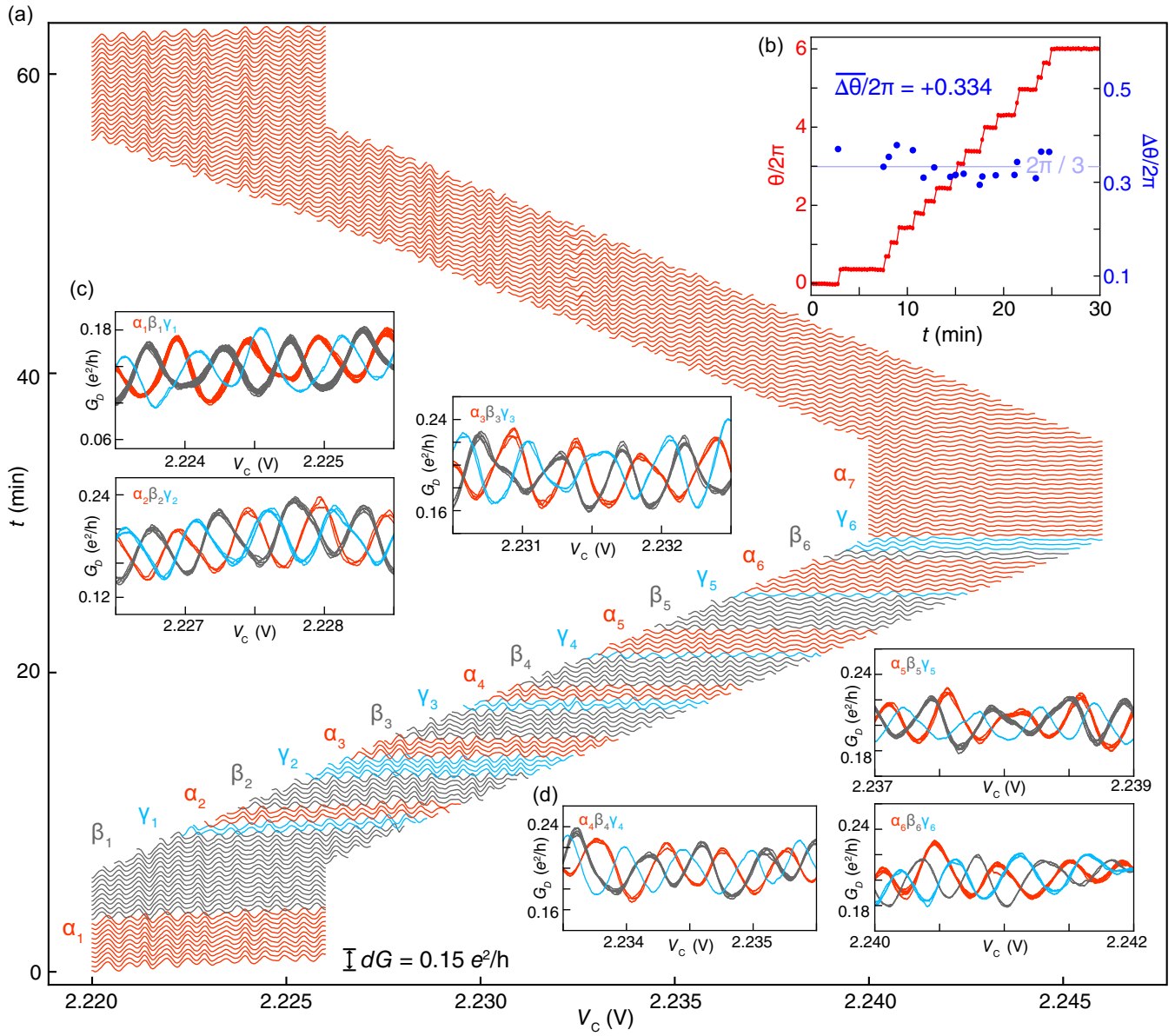

FIG. 5. Gate hysteretic phase slips at constant field. (a) Repeated line traces of the conductance G_D plotted as a function of V_C. Traces are vertically offset by an amount proportional to the time between the start of each trace. The window over which V_C is swept gradually increases over time, favoring an increase in the number of quasiparticles. Interpreting each phase slip as the addition of a single anyon, the traces are grouped into distinct classes α, β, and γ corresponding to the respective values of N_{qp} mod 3. No phase slips are seen as the gate voltage is swept back over the range in the reverse direction. (b) The phases extracted from the Fourier transform of each trace in (a) are plotted in red. Each phase jump is assumed to lie in the interval $(-\pi, \pi)$. Blue points correspond to the magnitude of each sudden jump in θ. (c),(d) Collections of line traces from each set of three adjacent classes $\alpha_i, \beta_i, \gamma_i$ plotted over the region where the data overlap in V_C. The stability of the phase is apparent given the overlap between traces within a given class, while the classes are offset from each other by a $\sim 2\pi/3$ phase shift.

over about one hour. Most successive traces show identical oscillatory patterns, but a pattern of abrupt phase slips is again evident. We label adjacent traces with the same phase with the same color, highlighting the stability of the phase over multiple scans. Notably, the apparent hysteresis in Fig. 5(a), while similar to that observed as a function of magnetic field, is even more extreme: A series of phase slips are visible for increasing V_C, but the phase remains perfectly stable as V_C is decreased back over the same range.

Figure 5(b) shows the phase θ of each trace extracted from the discrete Fourier transform. Notably, no background subtraction is necessary at constant B. We observe 18 phase slips over this range with a mean value of $2\pi \times 0.334$ and a standard deviation of $2\pi \times 0.038$. We interpret each of these slips as the entry of a single $e/3$

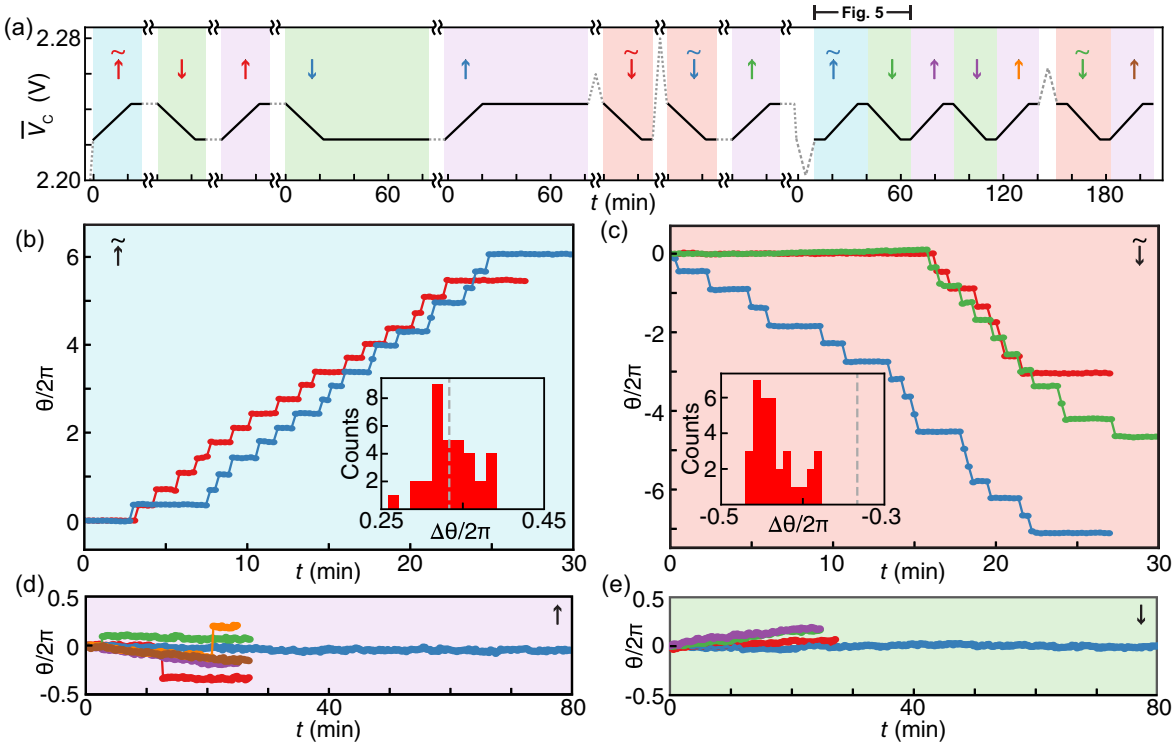

FIG. 6. Dependence of phase slip phenomenology on gate history. (a) Data are collected as the center gate voltage is ramped over a 6-mV-wide window centered at the value of $\bar{V}_C$ in the illustrated trajectory. (b) The phase extracted via FFT for sweeps of increasing $\bar{V}_C$ in which the measurement was preceded by an excursion to lower voltage outside the plateau ($\widetilde{\uparrow}$), (c) decreasing $\bar{V}_C$ in which the measurement was preceded by an excursion to higher voltage outside the plateau ($\widetilde{\downarrow}$), (d) increasing $\bar{V}_C$ in which the measurement was not preceded by an excursion to lower voltage (↑), and (e) decreasing $\bar{V}_C$ in which the measurement was not preceded by an excursion to higher voltage (↓). Differently colored data points correspond to different segments of the full sweep summarized in (a); data point colors correspond to each arrow labeling the respective sweep segment in (a). Insets in (b) and (c) show histograms of the values of the phase differences $\Delta\theta$ between plateaus of stable θ, with the gray dashed lines indicating $\Delta\theta = \pm 2\pi/3$. In (b), $\Delta\theta/2\pi = +0.336 \pm 0.03$, and in (c), $\Delta\theta = -0.434 \pm 0.03$.

quasiparticle into the interferometer (or the neutralization of a single $-e/3$ quasihole). We correspondingly collect traces into groups where the phase is the same, and label these by a Greek letter $\{\alpha, \beta, \gamma\}$ corresponding to N_{qp} mod 3. A numerical subscript distinguishes traces with the same N_{qp} mod 3 that are separated by three phase slips; assuming each phase slip corresponds to entry of a single fractionally charged quasiparticle, these traces correspond to charge configurations differing by an integer number of whole electron charges in the interferometer. Figures 5(c) and 5(d) compare traces $\{\alpha_i, \beta_i, \gamma_i\}$ for $i = \{1, \ldots, 6\}$. Each comparison shows a clear "triple-helix" pattern arising from the $2\pi/3$ relative phase shift between each set of curves.

The large hysteresis observed in Fig. 5 raises broader questions about the role of memory effects in quasiparticle dynamics and phase slip phenomenology. To investigate this, we perform repeated measurements following the protocol of Fig. 5, in which the interferometer phase is measured by rapid rastering of V_C in a small range while the center of this window, denoted $\bar{V}_C$, is slowly changed within the transport plateau. Besides performing multiple repetitions of the same trajectories, we also intersperse these measurements with "excursions" to either higher or lower $\bar{V}_C$ outside the transport plateau. This measurement protocol is shown in Fig. 6(a). During the intervals indicated by the solid black line, interferometeric phase data are collected continuously by rasterizing V_C while $\bar{V}_C$ is adjusted or held fixed. During the regions denoted by dotted black lines, $\bar{V}_C$ is either held constant or swept over the indicated range *without* taking interferometry data (in these dashed regions V_C is not rasterized). While these excursions are not precisely timed, they are typically several minutes in duration. The magnetic field and all other gate voltages are held constant for the entire course of the experiment. Repeated measurements of the interferometer phase in the same gate voltage regime $[\bar{V}_C \in (2.223, 2.243)]$ are color coded by two criteria: (1) whether they are measured for rising or falling $\bar{V}_C$ (and thus average ν) and (2) whether they are directly preceded by an excursion to large or small $\bar{V}_C$ before the falling or rising trajectories, respectively. We denote the

four scenarios by $\uparrow, \downarrow, \widetilde{\uparrow}, \widetilde{\downarrow}$, where the arrow indicates the sweep direction, and a wavy line indicates that the sweep was directly preceded by an excursion outside the transport plateau. Phase slip data for each of the resulting four sweep types are shown in Figs. 6(b)–6(e).

A striking pattern is evident in the presence or absence of phase slips for a given measurement. Specifically, multiple phase slips are observed consistently upon entry to the plateau from larger or smaller $\bar{V}_C$ (types $\widetilde{\uparrow}, \widetilde{\downarrow}$), but none are observed when the gate voltage direction is reversed within the plateau (types $\uparrow, \downarrow$). Consequently, multiple phase slips are observed for increasing $\bar{V}_C$ only on the first entry of the plateau from below [$\widetilde{\uparrow}$, Fig. 6(b)], but are observed for decreasing $\bar{V}_C$ only for the first entry of the plateau from above [$\widetilde{\downarrow}$, Fig. 6(c)]. With the exception of the occasional events observed in Fig. 6(d), slips are never observed upon repeated reversal within the plateau for either sweep direction ($\uparrow, \downarrow$) after the first sweep until the voltage is again swept well outside the central range.

The presence of hysteresis makes it clear that different microscopic charge configurations can be accessed at the same values of V_C depending on the history of the system. This is most obvious in the irreversible ratcheting of N_{qp}, which is consistent with a mobility gap near the plateau center where charge equilibration times become far larger than experimentally accessible. Less obvious is the fact that rising- and falling-bar $\bar{V}_C$ traces may access radically different charge configurations. The large excursions in $\bar{V}_C$ preceding a rising or falling trace will tend to heavily dope the interferometer; $\widetilde{\uparrow}$ sweeps thus begin from a state with many quasiholes while $\widetilde{\downarrow}$ begin with many quasiparticles. Owing to the presence of the mobility gap, $\widetilde{\downarrow}$ traces presumably correspond to removing quasiparticles from the heavily quasiparticle-doped $\nu = 1/3$ vacuum, while $\widetilde{\uparrow}$ traces correspond to removing quasiholes from the heavily quasihole-doped $\nu = 1/3$. The difference between these regimes is highlighted by the asymmetry in the experimentally determined phase slip magnitude. As shown in the insets of Figs. 6(b) and 6(c), while the phase slip magnitudes for $\widetilde{\uparrow}$ traces are clustered around the expected, quantized value $\Delta\theta = 2\pi/3$, for the $\widetilde{\downarrow}$ data the value is instead near $\Delta\theta/2\pi = -0.43$ [Fig. 6(c)]. Notably, the standard deviation of $\Delta\theta$ in Fig. 6(c), where the phase slips are not consistent with the expected quantized values, is no higher than in Fig. 2(a) or 6(b), where $\Delta\theta \approx 2\pi/3$.

The discrepancy between the observed phase slip magnitude for $\widetilde{\downarrow}$ and the expected quantized value calls into question the interpretation of these slips in terms of the anyon statistical phase θ_a. Deviation from a quantized value (e.g., $\theta_a = 2\pi/3$ for $e/3$ anyons, or $\theta_a = 2\pi$ for whole electrons) is most naturally accounted for by invoking bulk-edge coupling. We consider two scenarios. In the first, phase slips correspond to the changing the interferometer charge by $e/3$. In this case, the quantized phase slips observed for rising $\bar{V}_C$ correspond to addition of single anyons to states with negligible bulk-edge coupling, so that the entire phase slip is generated by θ_a. Decreasing $\bar{V}_C$ then must change the anyon number closer to the edge, where bulk-edge coupling effects are strong. Alternatively, the phase slips could be *entirely* generated by bulk-edge coupling as would be the case if each event corresponds to the addition of a whole electron, with no observable contribution from θ_a. In either scenario, the asymmetry in the measured values of $\Delta\theta$ indicates that the added charge induced for rising and falling $\bar{V}_C$ must occupy different orbital states with contrasting bulk-edge coupling.

Before analyzing these scenarios quantitatively, we note that the tight clustering of the observed phase slips' magnitudes already imposes constraints on the underlying microscopic picture. In particular, this observation is inconsistent with a picture where quasiparticles are added to pinning sites randomly distributed throughout the bulk, which would result in a large variation in the bulk-edge coupling and consequently the phase slip values. Instead, the tight clustering of phase slip values is more consistent with a picture where quasiparticles are added to a compressible "puddle" of charge, so that successive addition of quantized charges produces phase slips of nearly the same magnitude. Notably, our previous study of this regime at $\nu = -1$ in a device of similar construction found phase slips with magnitudes $\Delta\theta \leq 0.1$, considerably smaller than reported here [49].

The phenomenological theory of bulk-edge coupling [10] gives the phase slip magnitude $\Delta\theta$ in terms of the variables K_I and K_{IL}, which parametrize the energetic cost to add charge to the interferometer edge and the cross coupling between the edge and the bulk, as

$$\Delta\theta = 2\pi e^*(1 - K_{IL}/K_I). \tag{2}$$

where $e^* = q/e$. $K_I = hv_{\text{edge}}/\text{L}\nu$ can be determined by measuring the change in common mode voltage applied to both the source and drain electrodes simultaneously required to induce a $\Delta\theta = 2\pi$ phase shift; we find $K_I = 234$ μeV. K_{IL} can be estimated separately using a simple microscopic model of a compressible puddle, separated by a distance l from the edge state [47]. K_{IL} is maximal when the bulk puddle reaches all the way to the edge, and decreases with increasing separation between edge and bulk. Within this model, the upper bound on K_{IL} is half the charging energy of the interferometer bulk,

$$K_{IL} \leq \frac{1}{2}\frac{e^2}{C^g_{\text{bulk}}}, \tag{3}$$

where C^g_{bulk} is the total geometric capacitance of the interferometer bulk. We estimate $C^g_{\text{bulk}} \approx 2\epsilon A/d$, where d is the average distance to the gates and $\epsilon \approx 3.25\epsilon_0$ is the

c-axis dielectric constant of h-BN, from which we determine an upper bound, $K_{IL} \leq 80$ μeV.

Given our estimated K_I, then, K_{IL} may be determined from the measured $\Delta\theta$ to check if it is consistent with this bound. For the case of adding an integer electron charge, $q = e$, the measured $\Delta\theta/2\pi = 0.334$ and -0.434 give $K_{IL} = 155$ and 132 μeV, respectively, both of which violate the bound. Our data are thus incompatible with a model of a compressible puddle to which integer electron charges are added. Notably, this contrasts with a similar analysis of data from integer filling, where this model is found to be in agreement with observations [49].

In a picture where the compressible puddle is composed of $e/3$ quasiparticles, the quantized slips of Fig. 6(b) for the $\widetilde{\uparrow}$ data imply a negligible bulk-edge coupling. This is consistent with prior results at $\nu = -1$ [49], which found $(1 - K_{IL}/K_I) \approx 0.9$. Comparable bulk-edge coupling would lead to an expected $\Delta\theta \approx 0.3$ for anyons at $\nu = 1/3$. However, a crucial feature of the bulk-edge coupling is that in general it only *reduces* the observed phase slip magnitude associated with the entry of a single quasiparticle. Thus the phase slips with $\Delta\theta = -0.43$ in Fig. 6(c) for the $\widetilde{\downarrow}$ sweeps cannot be accounted for in a model where each slip corresponds to the addition of only one $e/3$ quasiparticle, even near the sample boundary.

Thus, while the nonquantized value implies that bulk-edge coupling must play a role in determining the phase slip magnitudes, it is also evident that neither a model based on whole-electron jumps nor single-$e/3$ quasiparticle jumps can account for the observed slips. This motivates consideration of alternative processes, such as those involving multiple quasiparticles. In particular, correlated dynamics—whereby quasiparticles may enter or exit in pairs—could give rise to phase slips with magnitudes distinct from those expected for individual particles. In the following section, we identify evidence for such processes by analyzing the fine structure of individual interference patterns—i.e., features beyond the primary phase—encoded in modulations of the fringe amplitudes.

IV. TIME-DOMAIN RECONSTRUCTION OF A $2e/3$ JUMP

Within an individual panel of Fig. 5(a), all curves are measured under identical conditions of magnetic field and applied gate voltages. As might be expected, traces taken at different times prior to a charging event show excellent reproducibility. A less obvious question is whether the addition of charge $q = e$ to the interferometer, particularly when it occurs deep in the bulk, modifies the $G_D - V_C$ relation even though no effect on the interferometer phase is expected. In Figs. 7(a)–7(c), we collect traces from the data of Fig. 5(a) which are separated by three quantized phase slips, and, indeed, see no discernible change in the oscillation *phase*. Notably, however, despite accumulating

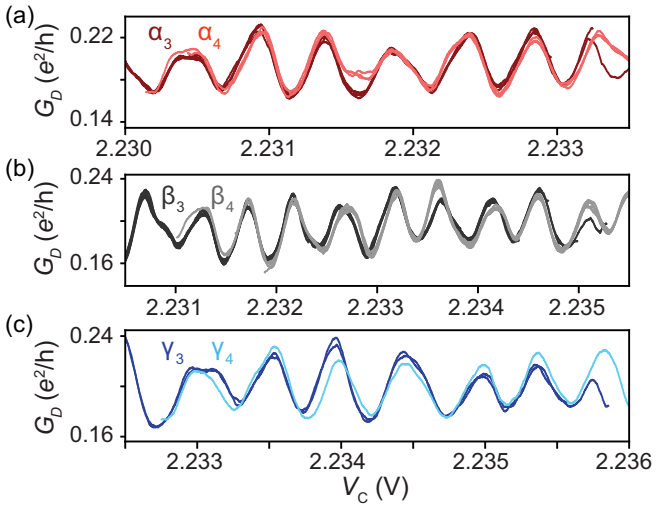

FIG. 7. Comparison of charge fingerprints for quantized phase slips. Traces are shown in the gate voltage range where they overlap, corresponding to the classes in Fig. 5(a) labeled (a) α_3 and α_4, (b) β_3 and β_4, and (c) γ_3 and γ_4.

$\Delta\theta = 2\pi$, traces which represent charge configurations differing by a whole electron—e.g., α_3 and α_4—remain distinguishable through deviations in the precise *amplitude* of individual interference fringes. This effect is robust across nearly all groups of traces separated by a 2π phase shift (see Supplemental Material for the complete set [47]). We speculate that this "charge fingerprint" encoded in the fringe intensities arises from the exponential sensitivity of transmission through our quantum point contacts to their electrostatic environment—including the electrical potential generated by the addition of even a gate-screened electrical charge in the bulk.

Regardless of microscopic origin, however, the pattern of oscillation amplitudes provides information about the charge configuration not contained in the oscillation phase alone. As a result, it allows us to extract information about the absolute phase (interpreted as the total electron charge in the interferometer [53]) rather than just the phase modulo 2π. This in turn allows us to resolve quasiparticle *entry* and *exit* under static experimental conditions in the time domain.

Figure 8(a) shows the result of ramping the magnetic field to a set point and then, starting from $t = 0$, leaving it constant for 35 min while continuing to repeatedly ramp V_C over a small (∼1.5 mV) range. Several phase slips are visible over the course of the experiment, separating regions of stable phase which we label I–VII in Fig. 8(b). If the phase jumps were assumed to fall into the interval $(-\pi, \pi)$, their nearly consistent magnitudes could lead to the conclusion that every jump corresponds to the addition of one quasiparticle, as is energetically favored by the reduction in total flux at the beginning of the measurement.

However, a close examination of the measured conductance [Fig. 8(b), insets] shows the fringe intensity patterns in

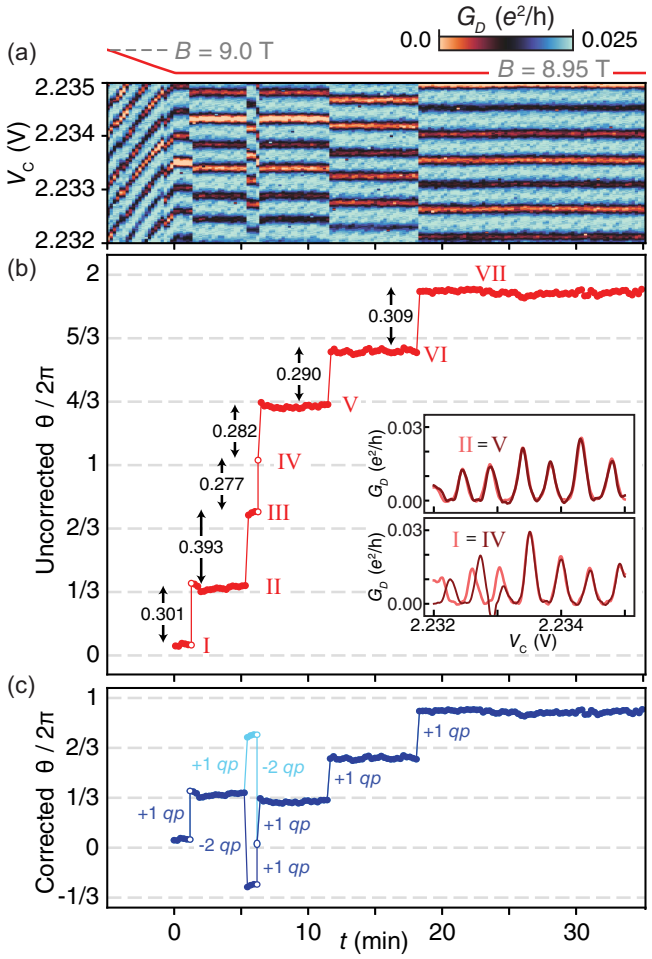

FIG. 8. Time-domain reconstruction of the quasiparticle occupation. (a) Repeated measurement of G_D over a fixed window of V_C. At the beginning of the measurement, the magnetic field is swept from 9.0 to 8.95 T, where it is subsequently held constant for 35 min. (b) The phase θ extracted from the Fourier transform of the data in (a). Each jump is assumed to be in the interval $\Delta\theta \in (-\pi, \pi)$. For traces in which a phase jump is observed in the middle of the line trace, two points are plotted as open circles, corresponding to the two values of phase extracted before and after the jump. Inset: G_D traces from regions II and V vs compared to line traces taken from regions I and IV. (c) Two versions of the corrected phase θ identical to (b) except with a shift of -2π applied to the jump from II to III (dark blue), or the jump from III to IV (light blue). Either modification would match the "charge fingerprints" of regions I and IV, and regions II and V.

regions II and V to be indistinguishable; regions I and IV are also identical after noting that the phase slip occurs midway through the single trace that comprises region IV. This leads us to identify these regions with a return to the same charge configuration as well as the same absolute phase. In fact, equating the regions which have an indistinguishable charge fingerprint necessitates that at least one of the first three phase slips must correspond to a *removal* of two quasiparticles, rather than the naive interpretation of every slip as the addition of a single quasiparticle. Figure 8(c) shows two possible corrected traces of $\theta(t)$, with the light and dark blue traces differing from the uncorrected θ by a shift of -2π at the second or third phase slip, respectively.

The time dependence of the quasiparticle number implied by either of these possibilities reconciles our earlier observation of the identical charge fingerprints in *both* regions I and IV, and regions II and V. The information required to discriminate between the two possibilities is provided by the magnitude of the phase slip from region II to region III: Here, $\Delta\theta$ is significantly *larger* than θ_a, whereas a finite amount of bulk-edge coupling should only serve to decrease the magnitude of the phase jump. (All of the other phase slips show a value slightly less than θ_a.) This suggests that the slip separating regions II and III should be associated with a decrease in the number of quasiparticles by two, as the change in phase is then $\Delta\theta = -4\pi/3 + \delta\theta_{\mathrm{BE}}$. In other words, we interpret $\Delta\theta/2\pi = 0.393 = -\frac{2}{3}(1 - K_{IL}/K_I) + 1$, which gives a value of $K_{IL}/K_I \approx 0.1$ consistent with small bulk-edge coupling.

In addition to the potential for such processes to account for the nonquantized phase slips from Fig. 5(c), we note that double-quasiparticle tunneling is not without precedent. Experimentally, an "Andreev-like" scattering process involving a charge-$2e/3$ excitation at the $\nu = 1/3$ edge has been observed in a $\nu = 1$ to $\nu = 1/3$ heterojunction [46], and shot noise measurements in the fractional quantum Hall regime have sometimes found evidence of cooperative tunneling of multiple quasiparticles [54–56]. Capacitive signatures have also revealed correlated double-electron additions to quantum dots in the integer quantum Hall regime [57]. Furthermore, recent theoretical work has suggested that the lowest energy multiquasiparticle configuration in some fractional quantum Hall systems may involve formation of "anyonic molecules" or clusters composed of two or more quasiparticles [58,59].

V. DISCUSSION

The exceptionally slow quasiparticle dynamics of our interferometer open new routes to quantitatively probe the physics of fractionalized phases at the single anyon level. Measuring few-anyon dynamical processes via the response of the interferometric phase to both θ_a and Coulomb effects may give new insight into states where interquasiparticle correlations are important, such as in the formation dynamics of Wigner crystal states, anyonic molecules, and the hierarchical fractional quantum Hall states.

Recent advances in spatial imaging techniques, allowing high resolution charge sensing in dual-gated devices [60], may be used to help resolve these questions. Applied to interferometer devices of a similar construction to ours, this may allow direct correlation between the real-space distribution of localized anyons and the interferometric phase. Graphene heterostructures also host even denominator

fractional quantum Hall states thought to support non-Abelian anyons [27,28,61]. In bilayer graphene, the energy gaps of these states are comparable to that of the $1/3$ state studied here [30,31], suggesting similarly slow dynamics for charge $e/4$ quasiparticles. A key open question is the timescale for motion of the charge-neutral excitations that encode fermion parity, which future experiments of this kind may help illuminate.

Note added—Recently, we became aware of related work using a similar graphene device [37].

ACKNOWLEDGMENTS

The authors acknowledge helpful discussions with T. Wang, S. Kivelson, and S. Das Sarma. Work at UCSB was primarily supported by the Office of Naval Research under Award No. N00014-23-1-2066. Development of fabrication based on anodic oxidation lithography was supported by the Air Force Office of Scientific Research under Award No. FA9560-20-1-0208. A. F. Y. acknowledges additional support by the Brown Investigator Award. L. A. C. and N. L. S. received additional support from the Army Research Office under Award No. W911NF20-1-0082. M. P. Z. was supported by the U.S. Department of Energy, Office of Science, Office of Basic Energy Sciences, Materials Sciences and Engineering Division under Contract No. DE-AC02-05-CH11231 (Theory of Materials program KC2301). K. W. and T. T. acknowledge support from JSPS KAKENHI (Grants No. 19H05790, No. 20H00354, and No. 21H05233).

DATA AVAILABILITY

The data that support the findings of this article are openly available [62].

[1] J. M. Leinaas and J. Myrheim, *On the theory of identical particles*, Il Nuovo Cimento B **37**, 1 (1977).
[2] G. A. Goldin, R. Menikoff, and D. H. Sharp, *Particle statistics from induced representations of a local current group*, J. Math. Phys. (N.Y.) **21**, 650 (1980).
[3] F. Wilczek, *Quantum mechanics of fractional-spin particles*, Phys. Rev. Lett. **49**, 957 (1982).
[4] D. Arovas, J. R. Schrieffer, and F. Wilczek, *Fractional statistics and the quantum Hall effect*, Phys. Rev. Lett. **53**, 722 (1984).
[5] B. I. Halperin, *Statistics of quasiparticles and the hierarchy of fractional quantized Hall states*, Phys. Rev. Lett. **52**, 1583 (1984).
[6] N. Read and S. Das Sarma, *Clarification of braiding statistics in Fabry–Perot interferometry*, Nat. Phys. **20**, 381 (2023).
[7] S. Kivelson, *Semiclassical theory of localized many-anyon states*, Phys. Rev. Lett. **65**, 3369 (1990).
[8] C. de C. Chamon, D. E. Freed, S. A. Kivelson, S. L. Sondhi, and X. G. Wen, *Two point-contact interferometer for quantum Hall systems*, Phys. Rev. B **55**, 2331 (1997).
[9] E.-A. Kim, *Aharanov-Bohm interference and fractional statistics in a quantum Hall interferometer*, Phys. Rev. Lett. **97**, 216404 (2006).
[10] B. I. Halperin, A. Stern, I. Neder, and B. Rosenow, *Theory of the Fabry-Perot quantum Hall interferometer*, Phys. Rev. B **83**, 155440 (2011).
[11] F. E. Camino, W. Zhou, and V. J. Goldman, *Realization of a Laughlin quasiparticle interferometer: Observation of fractional statistics*, Phys. Rev. B **72**, 075342 (2005).
[12] F. E. Camino, W. Zhou, and V. J. Goldman, *$e/3$ Laughlin quasiparticle primary-filling $\nu = 1/3$ interferometer*, Phys. Rev. Lett. **98**, 076805 (2007).
[13] Y. Zhang, D. T. McClure, E. M. Levenson-Falk, C. M. Marcus, L. N. Pfeiffer, and K. W. West, *Distinct signatures for Coulomb blockade and Aharonov-Bohm interference in electronic Fabry-Perot interferometers*, Phys. Rev. B **79**, 241304(R) (2009).
[14] D. T. McClure, Y. Zhang, B. Rosenow, E. M. Levenson-Falk, C. M. Marcus, L. N. Pfeiffer, and K. W. West, *Edge-state velocity and coherence in a quantum Hall Fabry-Pérot interferometer*, Phys. Rev. Lett. **103**, 206806 (2009).
[15] N. Ofek, A. Bid, M. Heiblum, A. Stern, V. Umansky, and D. Mahalu, *Role of interactions in an electronic Fabry–Perot interferometer operating in the quantum Hall effect regime*, Proc. Natl. Acad. Sci. U.S.A. **107**, 5276 (2010).
[16] H. K. Choi, I. Sivan, A. Rosenblatt, M. Heiblum, V. Umansky, and D. Mahalu, *Robust electron pairing in the integer quantum Hall effect regime*, Nat. Commun. **6**, 7435 (2015).
[17] I. Sivan, H. K. Choi, J. Park, A. Rosenblatt, Y. Gefen, D. Mahalu, and V. Umansky, *Observation of interaction-induced modulations of a quantum Hall liquid's area*, Nat. Commun. **7**, 12184 (2016).
[18] J. Nakamura, S. Fallahi, H. Sahasrabudhe, R. Rahman, S. Liang, G. C. Gardner, and M. J. Manfra, *Aharonov–Bohm interference of fractional quantum Hall edge modes*, Nat. Phys. **15**, 563 (2019).
[19] J. Nakamura, S. Liang, G. C. Gardner, and M. J. Manfra, *Direct observation of anyonic braiding statistics*, Nat. Phys. **16**, 931 (2020).
[20] J. Nakamura, S. Liang, G. C. Gardner, and M. J. Manfra, *Fabry-Pérot interferometry at the $\nu = 2/5$ fractional quantum Hall state*, Phys. Rev. X **13**, 041012 (2023).
[21] R. L. Willett, K. Shtengel, C. Nayak, L. N. Pfeiffer, Y. J. Chung, M. L. Peabody, K. W. Baldwin, and K. W. West, *Interference measurements of non-Abelian $e/4$ & Abelian $e/2$ quasiparticle braiding*, Phys. Rev. X **13**, 011028 (2023).
[22] J. Nakamura, S. Liang, G. C. Gardner, and M. J. Manfra, *Impact of bulk-edge coupling on observation of anyonic braiding statistics in quantum Hall interferometers*, Nat. Commun. **13**, 344 (2022).
[23] C. R. Dean, A. F. Young, P. Cadden-Zimansky, L. Wang, H. Ren, K. Watanabe, T. Taniguchi, P. Kim, J. Hone, and K. L. Shepard, *Multicomponent fractional quantum Hall effect in graphene*, Nat. Phys. **7**, 693 (2011).

[24] H. Polshyn, H. Zhou, E. M. Spanton, T. Taniguchi, K. Watanabe, and A. F. Young, *Quantitative transport measurements of fractional quantum Hall energy gaps in edgeless graphene devices*, Phys. Rev. Lett. **121**, 226801 (2018).

[25] Y. Zeng, J. I. A. Li, S. A. Dietrich, O. M. Ghosh, K. Watanabe, T. Taniguchi, J. Hone, and C. R. Dean, *High-quality magnetotransport in graphene using the edge-free Corbino geometry*, Phys. Rev. Lett. **122**, 137701 (2019).

[26] C. Dean, P. Kim, J. I. A. Li, and A. Young, *Fractional quantum Hall effects in graphene*, in *Fractional Quantum Hall Effects: New Developments* (World Scientific, Singapore, 2020), pp. 317–375.

[27] A. A. Zibrov, C. Kometter, H. Zhou, E. M. Spanton, T. Taniguchi, K. Watanabe, M. P. Zaletel, and A. F. Young, *Tunable interacting composite fermion phases in a half-filled bilayer-graphene Landau level*, Nature (London) **549**, 360 (2017).

[28] J. I. A. Li, C. Tan, S. Chen, Y. Zeng, T. Taniguchi, K. Watanabe, J. Hone, and C. R. Dean, *Even denominator fractional quantum Hall states in bilayer graphene*, Science **358**, eaao2521 (2017).

[29] A. A. Zibrov, E. M. Spanton, H. Zhou, C. Kometter, T. Taniguchi, K. Watanabe, and A. F. Young, *Even-denominator fractional quantum Hall states at an isospin transition in monolayer graphene*, Nat. Phys. **14**, 930 (2018).

[30] Y. Hu, Y.-C. Tsui, M. He, U. Kamber, T. Wang, A. S. Mohammadi, K. Watanabe, T. Taniguchi, Z. Papić, M. P. Zaletel, and A. Yazdani, *High-resolution tunnelling spectroscopy of fractional quantum Hall states*, Nat. Phys. **21**, 716 (2025).

[31] A. Assouline, T. Wang, H. Zhou, L. A. Cohen, F. Yang, R. Zhang, T. Taniguchi, K. Watanabe, Roger S. Mong, M. P. Zaletel, and A. F. Young, *Energy gap of the even-denominator fractional quantum Hall state in bilayer graphene*, Phys. Rev. Lett. **132**, 046603 (2024).

[32] C. Déprez, L. Veyrat, H. Vignaud, G. Nayak, K. Watanabe, T. Taniguchi, F. Gay, H. Sellier, and B. Sacépé, *A tunable Fabry-Pérot quantum Hall interferometer in graphene*, Nat. Nanotechnol. **16**, 555 (2021).

[33] Y. Ronen, T. Werkmeister, D. Haie Najafabadi, A. T. Pierce, L. E. Anderson, Y. J. Shin, S. Y. Lee, Y. H. Lee, B. Johnson, K. Watanabe, T. Taniguchi, A. Yacoby, and P. Kim, *Aharonov-Bohm effect in graphene-based Fabry-Pérot quantum Hall interferometers*, Nat. Nanotechnol. **16**, 563 (2021).

[34] L. Zhao, E. G. Arnault, T. F. Q. Larson, Z. Iftikhar, A. Seredinski, T. Fleming, K. Watanabe, T. Taniguchi, F. Amet, and G. Finkelstein, *Graphene-based quantum Hall interferometer with self-aligned side gates*, Nano Lett. **22**, 9645 (2022).

[35] H. Fu, K. Huang, K. Watanabe, T. Taniguchi, M. Kayyalha, and J. Zhu, *Aharonov–Bohm oscillations in bilayer graphene quantum Hall edge state Fabry–Pérot interferometers*, Nano Lett. **23**, 718 (2023).

[36] J. Kim, H. Dev, R. Kumar, A. Ilin, A. Haug, V. Bhardwaj, C. Hong, K. Watanabe, T. Taniguchi, A. Stern, and Y. Ronen, *Aharonov–Bohm interference and statistical phase-jump evolution in fractional quantum Hall states in bilayer graphene*, Nat. Nanotechnol. **19**, 1619 (2024).

[37] T. Werkmeister, J. R. Ehrets, M. E. Wesson, D. H. Najafabadi, K. Watanabe, T. Taniguchi, B. I. Halperin, A. Yacoby, and P. Kim, *Anyon braiding and telegraph noise in a graphene interferometer*, Science **388**, 730 (2025).

[38] L. A. Cohen, N. L. Samuelson, T. Wang, K. Klocke, C. C. Reeves, T. Taniguchi, K. Watanabe, S. Vijay, M. P. Zaletel, and A. F. Young, *Nanoscale electrostatic control in ultraclean van der Waals heterostructures by local anodic oxidation of graphite gates*, Nat. Phys. **19**, 1502 (2023).

[39] X.-G. Wen, *Edge transport properties of the fractional quantum Hall states and weak-impurity scattering of a one-dimensional charge-density wave*, Phys. Rev. B **44**, 5708 (1991).

[40] C. L. Kane and M. P. A. Fisher, *Transport in a one-channel Luttinger liquid*, Phys. Rev. Lett. **68**, 1220 (1992).

[41] P. Fendley, H. Saleur, and N. P. Warner, *Exact solution of a massless scalar field with a relevant boundary interaction*, Nucl. Phys. **B430**, 577 (1994).

[42] C. L. Kane and Matthew P. A. Fisher, *Impurity scattering and transport of fractional quantum Hall edge states*, Phys. Rev. B **51**, 13449 (1995).

[43] P. Fendley, A. W. W. Ludwig, and H. Saleur, *Exact conductance through point contacts in the $\nu = 1/3$ fractional quantum Hall effect*, Phys. Rev. Lett. **74**, 3005 (1995).

[44] F. P. Milliken, C. P. Umbach, and R. A. Webb, *Indications of a Luttinger liquid in the fractional quantum Hall regime*, Solid State Commun. **97**, 309 (1996).

[45] I. P. Radu, J. B. Miller, C. M. Marcus, M. A. Kastner, L. N. Pfeiffer, and K. W. West, *Quasi-particle properties from tunneling in the $\nu = 5/2$ fractional quantum Hall state*, Science **320**, 899 (2008).

[46] L. A. Cohen, N. L. Samuelson, T. Wang, T. Taniguchi, K. Watanabe, M. P. Zaletel, and A. F. Young, *Universal chiral Luttinger liquid behavior in a graphene fractional quantum Hall point contact*, Science **382**, 542 (2023).

[47] See Supplemental Material at http://link.aps.org/supplemental/10.1103/fwjg-mx9h for device fabrication details, QPC characterizations, measurements of the dc bias dependence of the interference, a model and quantitative estimation of the bulk-edge coupling, temperature dependence of the interference, an analysis of the uncertainty in the phase slip magnitudes, and additional data on the stability of the interference phase.

[48] T. Werkmeister, J. R. Ehrets, Y. Ronen, M. E. Wesson, D. Najafabadi, Z. Wei, K. Watanabe, T. Taniguchi, D. E. Feldman, B. I. Halperin, A. Yacoby, and P. Kim, *Strongly coupled edge states in a graphene quantum Hall interferometer*, Nat. Commun. **15**, 6533 (2024).

[49] N. L. Samuelson, L. A. Cohen, W. Wang, S. Blanch, T. Taniguchi, K. Watanabe, M. P. Zaletel, and A. F. Young, *Hard and soft phase slips in a Fabry-Pérot quantum Hall interferometer*, Phys. Rev. Lett. **134**, 256301 (2025).

[50] R. K. Goodall, R. J. Higgins, and J. P. Harrang, *Capacitance measurements of a quantized two-dimensional electron gas in the regime of the quantum Hall effect*, Phys. Rev. B **31**, 6597 (1985).

[51] J. P. Eisenstein, L. N. Pfeiffer, and K. W. West, *Negative compressibility of interacting two-dimensional electron and quasiparticle gases*, Phys. Rev. Lett. **68**, 674 (1992).

[52] F. Yang, A. A. Zibrov, R. Bai, T. Taniguchi, K. Watanabe, M. P. Zaletel, and A. F. Young, *Experimental determination of the energy per particle in partially filled Landau levels*, Phys. Rev. Lett. **126**, 156802 (2021).

[53] D. E. Feldman and B. I. Halperin, *Robustness of quantum Hall interferometry*, Phys. Rev. B **105**, 165310 (2022).

[54] E. Comforti, Y. C. Chung, M. Heiblum, V. Umansky, and D. Mahalu, *Bunching of fractionally charged quasiparticles tunnelling through high-potential barriers*, Nature (London) **416**, 515 (2002).

[55] A. Bid, N. Ofek, M. Heiblum, V. Umansky, and D. Mahalu, *Shot noise and charge at the* $2/3$ *composite fractional quantum Hall state*, Phys. Rev. Lett. **103**, 236802 (2009).

[56] B. Ghosh, M. Labendik, V. Umansky, M. Heiblum, and D. F. Mross, *Coherent bunching of anyons and dissociation in an interference experiment*, Nature (London) **642**, 922 (2025).

[57] A. Demir, N. Staley, S. Aronson, S. Tomarken, K. West, K. Baldwin, L. Pfeiffer, and R. Ashoori, *Correlated double-electron additions at the edge of a two-dimensional electronic system*, Phys. Rev. Lett. **126**, 256802 (2021).

[58] M. Gattu and J. K. Jain, *Molecular anyons in the fractional quantum Hall effect*, Phys. Rev. Lett. **135**, 236601 (2025).

[59] Q. Xu, G. Ji, Y. Wang, H. Q. Trung, and B. Yang, *Dynamics of anyon clusters in fractional quantum Hall fluids*, Phys. Rev. B **112**, 235112 (2025).

[60] H. Li, S. Li, E. C. Regan, D. Wang, W. Zhao, S. Kahn, K. Yumigeta, M. Blei, T. Taniguchi, K. Watanabe, S. Tongay, A. Zettl, M. F. Crommie, and F. Wang, *Imaging two-dimensional generalized Wigner crystals*, Nature (London) **597**, 650 (2021).

[61] D.-K. Ki, V. I. Fal'ko, D. A. Abanin, and A. F. Morpurgo, *Observation of even denominator fractional quantum Hall effect in suspended bilayer graphene*, Nano Lett. **14**, 2135 (2014).

[62] N. Samuelson, L. Cohen, W. Wang, S. Blanch, T. Taniguchi, K. Watanabe, M. Zaletel, and A. Young, *Slow quasiparticle dynamics and anyonic statistics in a fractional quantum hall Fabry-Perot interferometer*, Zenodo (2026), https://zenodo.org/records/18371748.